Technetium-99m-Galactosyl-Neoglycoalbumin Combined with Iodine-123-Tyr-(A14)-Insulin Visualizes Human Hepatocellular Carcinomas

Amir Kurtaran, Shu-Ren Li, Markus Raderer, Maria Leimer, Christian Müller, Johann Pidlich, Nikolaus Neuhold, Peter Hübsch, Peter Angelberger, Werner Scheithauer and Irene Virgolini

Departments of Nuclear Medicine, Oncology, Gastroenterology, Pathology, Radiology and Clinical Pharmacology, University of Vienna, Vienna, Austria; and Department of Radiochemistry, Research Center Seibersdorf, Austria

Human hepatocellular carcinoma (HCC) is the most frequent primary hepatic malignancy and its diagnosis by conventional methods is still difficult. We hypothesized that the expression of specific receptors could possibly be used to improve in vivo localization of HCC with specific receptor-based radioligands. **Methods:** In initial in vitro studies, receptor binding of ^{99m}Tc-galactosyl-neoglycoalbumin (^{99m}Tc-NGA) and ^{123}I-Tyr-(A14)-insulin to HCC was investigated. Scintigraphy was performed in 45 patients with histologically confirmed HCC using either ^{99m}Tc-NGA (75–150 MBq; 25–50 nmole, n = 27) and/or ^{123}I-Tyr-(A14)-insulin (100–150 MBq; 7.5–10 μg, n = 30). **Results:** HCC (1256 ± 290 pmole bound/mg protein, K_d = 3.4 ± 2.9 n*M*) expressed a 1000-fold higher number of specific receptors for ^{123}I-Tyr-(A14)-insulin compared to normal liver tissue (2.4 ± 0.8 pmole bound/mg protein, K_d = 4.2 ± 2.4 n*M*), whereas HCC did not express receptors specific for ^{99m}Tc-NGA. All HCC lesions were identified as cold spots after injection of ^{99m}Tc-NGA, whereas ^{123}I-Tyr-(A14)-insulin accumulated in these lesions, indicating HCC-to-normal liver ratios of 1.6 ± 0.4 in the mean. Subtraction images obtained from planar studies visualized ^{123}I-Tyr-(A14)-insulin in HCC lesions detected by ^{99m}Tc-NGA as cold spots. **Conclusion:** This hepatocyte receptor-specific, double-tracer method using ^{99m}Tc-NGA and ^{123}I-Tyr-(A14)-insulin could become clinically useful in the diagnosis of HCC.

Key Words: iodine-123-Tyr-(A14)-insulin; technetium-99m-galactosyl-neoglycoalbumin; hepatocellular carcinomas

J Nucl Med 1995; 36:1875–1881

In recent years, receptor-based radiopharmaceuticals have been used for localization diagnosis of certain tumors. For instance, radiolabeled octreotide (*1*) or vasoactive intestinal peptide (*2*) have been used to localize endocrine tumors or adenocarcinomas. Several hepatocyte receptor-seeking ligands have also been developed. Technetium-99m-galactosyl-neoglycoalbumin (^{99m}Tc-NGA) is one of these ligands that maintains specific and exclusive binding to the hepatic binding protein (HBP) receptor residing at the cell surface membrane of hepatocytes (*3*). Technetium-99m-NGA scanning was successfully applied for the evaluation of liver morphology as well as liver functional capacity (*4–9*). Also insulin recognizes abundant numbers of specific receptors at hepatocytes, suggesting the use of ^{123}I-Tyr-(A14)-insulin for in vivo liver scintigraphy (*10–12*). In addition, insulin was shown to stimulate the growth of normal and malignant cells (*13,14*).

Hepatocellular carcinoma (HCC) is one of the most common cancers in men with highly uneven geographic distribution. Whereas its worldwide annual incidence has been estimated to be 250,000 to 1 million (*15*), it accounts for only 1.5% of all cancers and to approximately 16,000 deaths in the United States (*16*). There is a well known relationship of HCC with prior hepatitis B and C viral infections (*15,17,18*) and a preponderance in men, with a male-to-female ratio of about 4:1 (*15,19*). Additional etiologic factors have also been discussed (*15*). A number of imaging modalities are used to detect HCC, but, radionuclide scanning techniques currently play only a minor role in the diagnosis of HCC (*20*). In an approach to visualize HCC, we used two specific hepatocyte receptor-seeking radioligands, ^{99m}Tc-NGA and ^{123}I-Tyr-(A14)-insulin.

METHODS

Radioiodination of Insulin

Insulin (NOVO Nordisk, Copenhagen, DK) was radioiodinated using the lactoperoxidase method as previously described (*10,12*). A specific activity of about 150 MBq/10 μg (i.e., 1 IU) ^{123}I-Tyr-(A14)-insulin was prepared. Briefly, to a polypropylene microvial were added 116 μg purified human insulin in 30 μl 0.01 *M* HCl, 30 μl 0.1 *M* Na-phosphate buffer, pH 7, about 400 MBq [^{123}I]NaI in 0.02 *M* NaOH (30 μl), 340 ng (=10 nmole) H_2O_2 in 10 μl H_2O and 10 μg lactoperoxidase in 10 μl H_2O. The reaction mixture was slowly vortexed for 5 min. Isolation and purification were performed by direct preparative high-performance liquid chromatography (HPLC) (reversed-phase; column: Nucleosil 100 C-18, 5 μm, 4 × 290 mm (Machery & Nagel, Düren, Germany); eluant: 70% (v/v) aqu. 0.2 *M* NH_4OAc, 0.01 *M* phosphate pH 3, 20%

Received Sept. 27, 1994; revision accepted May 15, 1995.

For correspondence or reprints contact: Irene Virgolini, MD, Department of Nuclear Medicine, University of Vienna, AKH, Währinger Gürtel 18-20, A-1090 Vienna, Austria.

CH_3CN, 10% i-propanol; flow 1 ml/min) of the reaction mixture. The ^{123}I-Tyr-(A14)-insulin peak was collected into a vial containing 1 mg human serum albumin (HSA) and was vacuum-evaporated to about 100 μl. After dilution with phosphate-buffered saline (PBS) containing 0.5% HSA, the final product was filtered through a low-protein adsorption membrane. Product identity and radiochemical purity (>98% in all preparations) was inherently established by high-resolution HPLC using a ^{125}I-Tyr-(A14)-insulin standard (Amersham International, Buckinghamshire, UK) and a separate analytical HPLC (identical to the preparative HPLC system) for analysis. Free iodide was additionally quantified by cellulose acetate electrophoresis and amounted to less than 1% determined 20 hr after labeling. Isolated radiochemical yield of ^{123}I-Tyr-(A14)-insulin in the HPLC peak (retention time 23.3 min) was about 50% (the other 50% was the sum of inorganic iodine species (3.2 min), ^{123}I-Tyr-(A19)- (11.2 min), ^{123}I-Tyr-(B26)- (20.7 min), ^{123}I-Tyr-(B16)- (21.5 min) and $^{123}I_2$Tyr-insulin (30.6 min), in order of elution.

Preparation and Labeling of NGA

Synthesis of NGA was done as described previously (*6–9*). Briefly, D(+)-galactose was acetylated and brominated to aceto-bromo-galactose and reacted to tetra-acetyl-β-D-galactosyl-thio-pseudourea which, by reaction with chloroaceto-nitrile, formed cyanomethyl-2,3,4,6-tetra-O-acetyl-β-D-thiogalactose (A). A solution of 0.1 *M* of (A) and 0.01 *M* CH_3ONa in absolute methanol was used as stock solution containing an average of 0.055 *M* 2-imino-2-methoxyethyl-1-thio-β-D-galactose (B, coupling reagent). An aliquot of B (125 μl; 0.055 *M*) was evaporated to dryness and redissolved in fresh 0.2 *M* borate buffer (pH 8.6). A precise amount of HSA was added and incubated overnight at room temperature to produce the final NGA ligand. NGA was routinely isolated by repetitive ultrafiltration through the membrane with a 20-kD exclusion limit separating unbound coupling agent into the filtrate. A molar ratio of coupling agent/HSA of 138 was used, resulting in about 21 galactose residues per HSA molecule. NGA was labeled with ^{99m}Tc to yield a specific activity of 150 MBq/50 nmole NGA. The final ^{99m}Tc-NGA preparation was filtered through a sterile 0.2-μm membrane. Radiochemical purity was routinely monitored by cellulose-acetate electrophoresis in 0.1 *M* barbital buffer (pH 8.6) run at 300 V for 20 min and was >97%. The labeling yield after filtration amounted to about 95%; the in vitro stability at room temperature exceeded 24 hr.

In Vitro Binding Studies

Preparation of HCC Tissue Homogenates. The HCC and normal liver specimens were obtained from six patients at surgery and immediately frozen under liquid nitrogen. Diagnosis was confirmed by histopathology. Tumor cell membrane fractions were prepared according to established techniques (*7,21*). Tissue was cut into pieces, put into 50 m*M* Tris HCl buffer, pH 7.5, and homogenized by ultrasound-turrax. The cell homogenate was centrifuged at 5000 g for 10 min at 4°C, washed and resuspended in assay buffer containing 50 m*M* Tris HCl, pH 7.5, 5 m*M* $MgCl_2$, 1 m*M* $CaCl_2$ and 0.1 *M* NaCl at a concentration of 100 μg protein/ml.

The conditions of the assay system were essentially the same as reported earlier (*21*). In initial experiments, the time course of association of binding as well as the temperature dependency were studied, indicating that equilibrium of binding was reached after a 30-min incubation time at 4°C. In saturation experiments, the membrane fractions were incubated with increasing concentrations of labeled ligand (0.01–100 n*M*) in absence (total binding) or presence of the same unlabeled ligand (100 n*M*, nonspecific binding). In competition experiments, the membrane fractions were incubated with 5 n*M* labeled ligand in absence (total binding) and presence of increasing concentrations (0.001–1000 n*M*) of the same unlabeled ligand. After incubation for 45 min at 4°C, the reaction mixture was diluted 1:10 with assay buffer and rapidly centrifuged (5000 g, 10 min, 4°C) to separate membrane-bound from free ligand. The resulting pellet was washed twice with assay buffer and counted in a gamma counter for 1 min. Specific binding was determined as the difference of total and nonspecific binding. Binding data were calculated according to Scatchard (*22*) using the Ligand program.

Patients

Fifty-seven consecutive patients were analyzed in this study. Forty-five patients had histologically verified HCC. Six patients with liver metastases spread from intestinal adenocarcinomas, four patients with liver cirrhosis and two patients with benign cystic liver adenomas served as controls (n = 12). Histopathology was obtained from biopsy material or at surgery. The location of the carcinomas was established by CT and/or US. All patients undergoing ^{123}I-Tyr-(A14)-insulin receptor scanning received sodium perchlorate (3 × 400 mg) for thyroid gland blockage starting 1 day before the injection.

Initially, either NGA (n = 15) or insulin (n = 10) receptor scanning was performed to explore both scintigraphic methods. In the next study phase, both scans were performed in the same patients within 1 to 6 wk between the imaging sessions (n = 5). Finally, the imaging protocol allowed injection of both tracers in a single study (n = 15) as described below. The control subjects also received both tracers in a single study.

Gamma Camera Imaging

The patients were positioned supine under a gamma camera equipped with a general-purpose, low-energy collimator (140 keV). In initial studies of both ^{99m}Tc-NGA and ^{123}I-Tyr-(A14)-insulin, dynamic imaging was performed at a rate of two frames per minute and a matrix of 128 × 128 pixels over a region covering the liver and heart. Total acquisition time was 30 min. If indicated, SPECT (matrix size 128 × 128 pixels, 360° (6°/step) rotation) acquisitions of the liver were performed after completion of the dynamic study.

In 20 of the 45 patients with HCC (8 women, 12 men, aged 46–78 yr, Table 1) both ^{99m}Tc-NGA and ^{123}I-Tyr-(A14)-insulin receptor scanning were performed. In five of these patients, sequential anterior scans were recorded, allowing a time interval of 6 wk maximum between both investigations. In the other 15 patients, as well as in the 12 control subjects, both ligands were applied in a single study. In these patients, 300K cts were acquired after injection of ^{99m}Tc-NGA in an anteroposterior view and ^{123}I-Tyr-(A14)-insulin was intravenously injected while the patient remained in the same supine position. Gamma camera acquisition was then performed for additional 300K cts. Subtraction images and ROIs were obtained using standard Toshiba (Tokyo, Japan) software.

Statistical Analysis

Statistical comparison between the means was made with the Student's t-test for unpaired data at a confidence level of 95%. Values are presented as means ± s.d.

TABLE 1
Technetium-99m-NGA/Iodine-123-Tyr-(A14)-Insulin Receptor Imaging of HCC

Patient no.	Sex	Age (yr)	CT/US findings	^{99m}Tc-NGA	^{123}I-Tyr-(A14)-insulin
1	M	66	Multiple lesions in segments II, III, IV, VII and VIII	Cold spots in all segments	Accumulation in all segments
2	M	78	Two lesions in segments VII and VIII	Cold spots in both segments	Accumulation in both segments
3	M	64	Multiple lesions in segments V, VI, VII and VIII	Cold spots in all segments	Accumulation in all segments
4	F	68	Single lesion in segment VII	Cold spot in this segment	Accumulation in this segment
5	M	59	Two lesions in segments VII and VIII	Cold spots in both segments	Accumulation in both segments
6	F	52	Two lesions in segments V and VI	Cold spots in both segments	Accumulation in both segments
7	F	64	Two lesions in segments V and VII	Cold spots in both segments	Accumulation in both segments
8	M	53	Single lesion in lobus quadratus	Cold spot in this area	Accumulation in this area
9	F	56	Single lesion in segment VII	Cold spot in this segment	Accumulation in this segment
10	M	65	Two lesions in segments IV and VI	Cold spots in both segments	Accumulation in both segments
11	M	51	Single lesion in segment VII	Cold spot in this segment	Decreased accumulation in this segment
12	F	67	Two lesions in segments V and VIII	Cold spots in both segments	Accumulation in both segments
13	F	65	Multiple lesions in segments IV and VII and VIII	Cold spots in all segments	Accumulation in all segments
14	M	46	Two lesions in segments V and VIII	Cold spots in both segments	Accumulation in segment V, decreased accumulation in segment VIII
15	M	69	Multiple lesions in segments V, VII and VIII	Cold spots in all segments	Accumulation in all segments
16	F	72	Multiple lesions in segments IV, VII, VIII	Cold spots in all segments	Accumulation in all segments
17	M	64	Two lesions in segments VI and VII	Cold spots in both segments	Accumulation in both segments
18	F	59	Single lesion in segment VII	Cold spot in this segment	Accumulation in this segment
19	M	78	Two lesions in segments VII and VIII	Cold spots in both segments	Accumulation in both segments
20	M	70	Two lesions in segments V and VIII	Cold spots in both segments	Accumulation in both segments

Patients 1–5 underwent dynamic acquisitions. Patients 6–20, after identification of cold spots on ^{99m}Tc-NGA images in the anteroposterior view, had ^{123}I-Tyr-(A14)-insulin imaging. Significant ^{123}I-Tyr-(A14)-insulin accumulation was demonstrated in 18 of 20 patients.

RESULTS

In Vitro Binding of Iodine-123-Tyr-(A14)-Insulin and Technetium-99m-NGA to Normal Liver and HCC Tissue

For normal liver cell homogenates, specific and saturable binding was obtained for both ^{123}I-Tyr-(A14)-insulin and ^{99m}Tc-NGA. Scatchard plot analysis of the saturation data indicated a single class of high affinity binding sites for ^{123}I-Tyr-(A14)-insulin (Fig. 1) and a high- and low-affinity binding class for ^{99m}Tc-NGA (*6,7*). On HCC, a remarkably higher number of specific ^{123}I-Tyr-(A14)-insulin receptors was identified, whereas virtually no binding of ^{99m}Tc-NGA in HCC was observed. The respective binding data were 2.4 ± 0.8 pmole ^{123}I-Tyr-(A14)-insulin/mg protein for normal liver tissue (K_d 4.2 ± 2.4 n*M*, IC_{50} for unlabeled insulin 8.3 ± 3.9 n*M*) and 1256 ± 290 pmole ^{123}I-Tyr-(A14)-insulin/mg protein of HCC tissue ($p < 0.001$; K_d 3.4 ± 2.9 n*M*; IC_{50} for unlabeled insulin 6.9 ± 3.0 n*M*). Normal liver bound 0.78 ± 0.2 pmole ^{99m}Tc-NGA/mg protein with high affinity (K_d 1.4 ± 0.7 n*M*) and 5.2 ± 1.8 pmole ^{99m}Tc-NGA/mg protein with low affinity (K_d 14.4 ± 4.6 n*M*). The IC_{50} for unlabeled NGA amounted to 21.7 ± 5.2 n*M*. For HCC

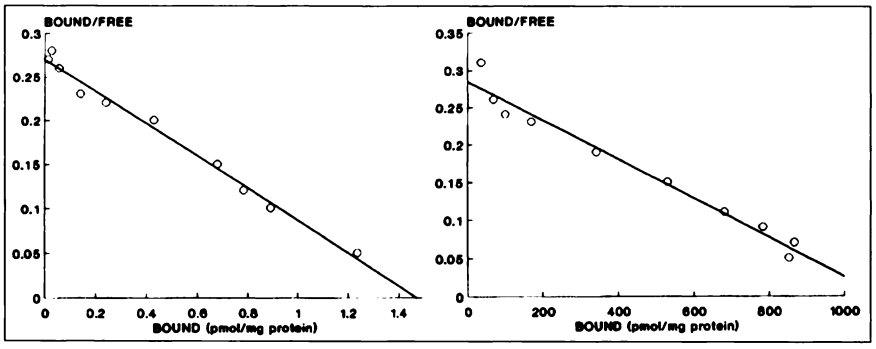

FIGURE 1. In vitro binding of ^{123}I-Tyr-(A14)-insulin to normal liver (left) and HCC tissue (right). Iodine-123-Tyr-(A14)-insulin bound to both normal liver and HCC tissue. Scatchard analyses indicated a B_{max} (maximal binding capacity) of 1.4 pmole/mg protein for normal liver and of 1078 pmole/mg protein for HCC tissue, corresponding K_d values were 3 and 4 n*M*, respectively.

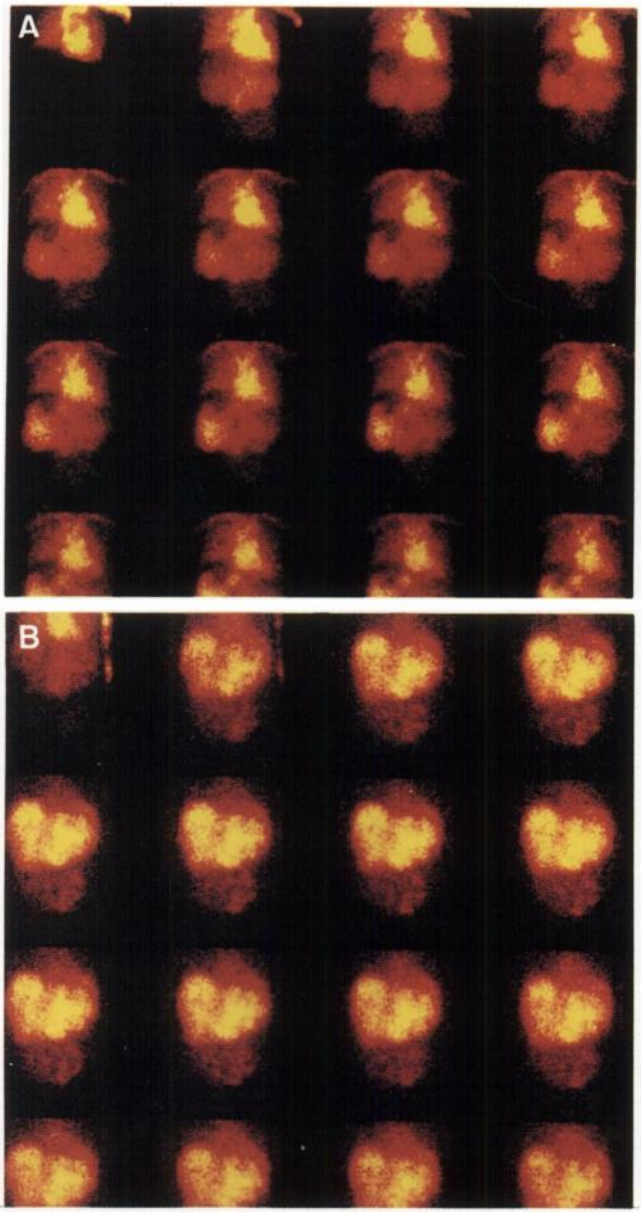

FIGURE 2. Visualization of multiple HCC lesions with ^{99m}Tc-NGA and ^{123}I-Tyr-(A14)-insulin in Patient 1. (A) After intravenous injection of ^{99m}Tc-NGA (150 MBq, 50 nmole NGA, the receptor tracer was rapidly trapped by normal human liver, whereas the HCC lesions appeared as clear cold spots in segments II, III, IV, VII, VIII. (B) Iodine-123-Tyr-(A14)-insulin (150 MBq, 10 μg insulin) bound to all NGA-indicated HCC lesions.

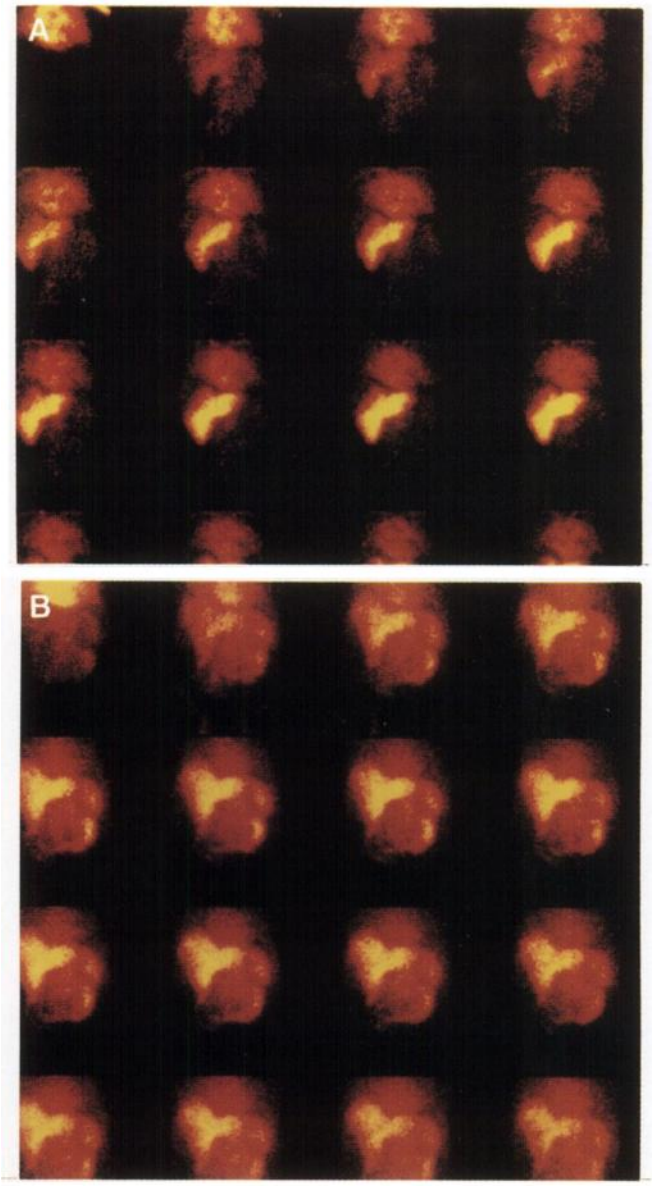

FIGURE 3. Visualization of a single HCC lesion with ^{99m}Tc-NGA and ^{123}I-Tyr-(A14)-insulin in Patient 2. Immediately after intravenous injection of ^{99m}Tc-NGA (150 MBq, 50 nmole NGA), the HCC lesion was indicated by a single cold spot in segments VII/VIII of the liver (A). Iodine-123-Tyr-(A14)-insulin (150 MBq; 10 μg insulin) produced significant in vivo binding to the same HCC lesion (B).

tissue, no specific binding of ^{99m}Tc-NGA was observed within the ligand ranges investigated (7).

In Vivo Binding of Technetium-99m-NGA

NGA scintigraphy was performed in 27 patients with HCC. HCC lesions were present in multiple sites in 19 patients and in a single site in 8 patients.

The liver was the only organ to accumulate ^{99m}Tc-NGA. In all patients, cold spots were demonstrated after ^{99m}Tc-NGA injection in CT/US visualized tumor lesions (Figs. 2, 3).

In Vivo Binding of Iodine-123-Tyr-(A14)-Insulin

Iodine-123-Tyr-(A14)-insulin scintigraphy was performed in 30 patients with HCC. HCC lesions were present in multiple sites in 18 patients and in single site in 12 patients.

After injection of ^{123}I-Tyr-(A14)-insulin, accumulation of the receptor tracer was found in CT/US and NGA-verified HCC lesions (Figs. 2–3). On average, the insulin uptake calculated for tumor lesions was higher compared to surrounding normal liver. In the mean, the HCC-to-normal liver ratios amounted to 1.6 ± 0.4 at peak maximum (6–10 min). This demonstrates increased uptake of ^{123}I-Tyr-

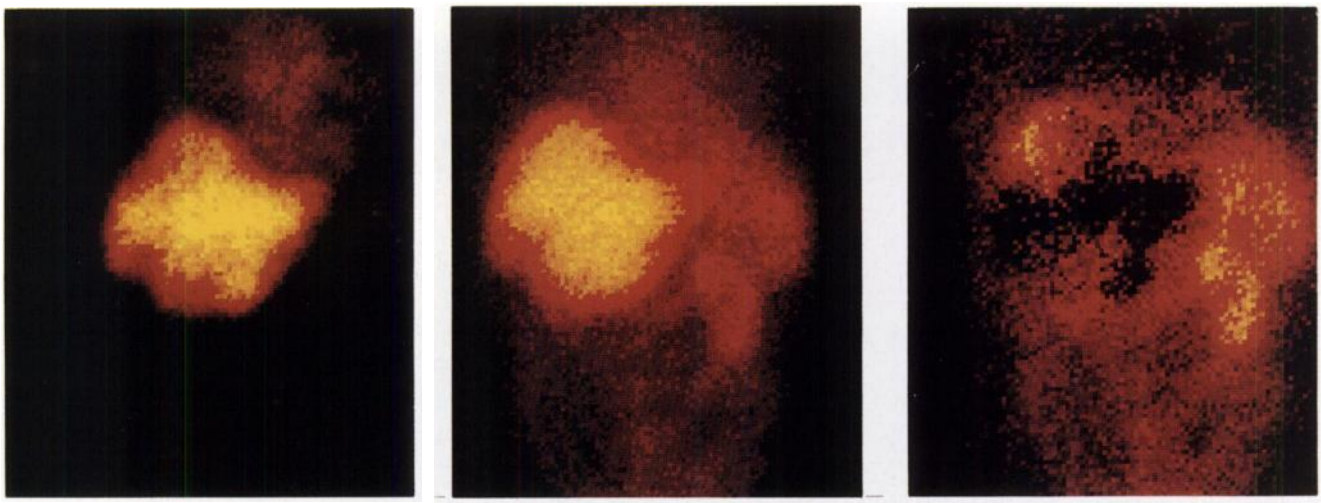

FIGURE 4. Visualization of two HCC lesions by substraction scintigraphy in Patient 7. Ten minutes after injection of 75 MBq ^{99m}Tc-NGA (25 nmole) static anterior imaging was performed. Two HCC lesions were indicated in segments VII and V (A). Fifteen minutes after start of the study, ^{123}I-Tyr-(A14)-insulin (100 MBq, 10 μg) was injected and another anterior static acquisition was performed in the same position. Iodine-123-Tyr-(A14)-insulin bound to both HCC lesions (B). After subtraction of ^{99m}Tc-NGA obtained from ^{123}I-Tyr-(A14)-insulin, remaining radioactivity located both HCC lesion sites (C).

(A14)-insulin by HCC and, thus, increased receptor binding. Individual patient data, however, indicated that in 19/30 patients significantly increased HCC-to-normal liver ratios were found (1.9 ± 0.4), in 8 patients HCC uptake of ^{123}I-Tyr-(A14)-insulin was not different to the surrounding normal liver (1.1 ± 0.2) and in 3 patients HCC uptake of ^{123}I-Tyr-(A14)-insulin was decreased (0.7, 0.8 and 0.9, respectively).

Dual Hepatocyte-Specific Receptor Imaging: Labeled Insulin and NGA Subtraction Study

Twenty patients (6 patients with liver metastases spread from intestinal adenocarcinomas, 4 patients with liver cirrhosis and 2 patients with benign liver adenomas) and 12 control subjects had both ^{99m}Tc-NGA and ^{123}I-Tyr-(A14)-insulin receptor-studies. In five of these patients, dynamic studies indicated a mismatch of the scan results (Figs. 2 and

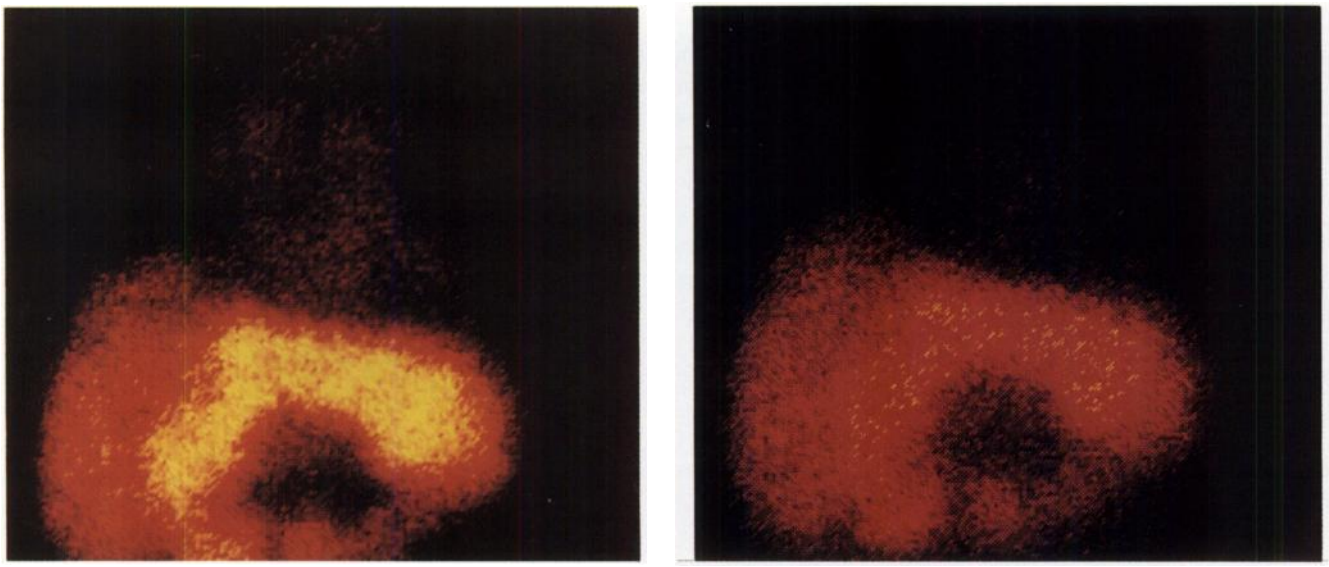

FIGURE 5. Technetium-99m-NGA and ^{123}I-Tyr-(A14)-insulin scanning in a patient with a single liver metastasis spread from an intestinal adenocarcinoma. Ten minutes after injection of ^{99m}Tc-NGA (75 MBq, 25 nmole), static anterior imaging was performed. Two large metastatic adenocarcinoma lesions were visualized as cold spots in segments IV/V and VII (A). Fifteen minutes after the start of the study, ^{123}I-Tyr-(A14)-insulin (100 MBq; 10 μg) was injected and anterior static acquisition was performed. In contrast to HCC lesions, ^{123}I-Tyr-(A14)-insulin did not accumulate in metastatic adenocarcinoma lesions (B).

3), i.e., cold spots after ^{99m}Tc-NGA injection and significant accumulation of ^{123}I-Tyr-(A14)-insulin.

In the other 15 patients as well as in all 12 control subjects, both ligands were applied in a single study. After identification of cold spots during ^{99m}Tc-NGA scanning, ^{123}I-Tyr-(A14)-insulin was injected while the patient was still in the same supine position under the gamma camera. In 13 of these patients, each of the HCC lesions detected as cold spots during ^{99m}Tc-NGA scanning showed significant accumulation of ^{123}I-Tyr-(A14)-insulin. As shown in Figure 4, subtraction of ^{99m}Tc-NGA from ^{123}I-Tyr-(A14)-insulin images indicated increased insulin receptor binding to HCC lesions. In the control subjects, however, cold spots observed on ^{99m}Tc-NGA scans were not concentrated on ^{123}I-Tyr-(A14)-insulin images (Fig. 5).

DISCUSSION

In this study, we report excellent visualization of histologically verified HCC using ^{99m}Tc-NGA and ^{123}I-Tyr-(A14)-insulin. HCC lesions were visible as cold spots on ^{99m}Tc-NGA scanning and concentrated radioactivity after injection of ^{123}I-Tyr-(A14)-insulin. Specificity of this dual-receptor tracer scanning procedure was documented by no accumulation of ^{123}I-Tyr-(A14)-insulin in cold spots visualized on NGA scans in hepatic metastases spread from adenocarcinomas, cirrhotic livers or cystic benign liver adenomas.

Technetium-99m-NGA was introduced to assess functional hepatic mass in addition to liver morphology and is specific for the hepatic binding protein (HBP) receptor which resides at the plasma membrane of hepatocytes (*3*). Therefore, the liver is the only tissue which selectively accumulates ^{99m}Tc-NGA after intravenous injection. Technetium-99m-NGA provided excellent hepatic images in all patients immediately after injection. We found that hepatomas do not express HBP receptor sites in vitro; this lack of sites was obviously responsible for the appearance of cold spots in the NGA images. This technique also has a similar limitation for hepatoma detection as compared with conventional ^{99m}Tc-sulfur colloid liver imaging, which has been the method of choice for the initial evaluation of HCC, as it is a sensitive but nonspecific screening test (*16,23,24*). As with ^{99m}Tc-sulfur colloid scanning, whenever a defect is detected on ^{99m}Tc-NGA images, another study is needed to characterize the cold nodule to increase the diagnostic accuracy of liver scan since the nodule could be a cyst, neoplasm, anatomical variant or some other condition. It was suggested that subtraction images obtained of colloid from a ^{67}Ga-citrate scan (*25,26*) might increase the specificity for detection of mismatched lesions which could be indicative of HCC. Subsequent studies, however, have shown that one-third of hepatomas fail to show selective uptake of ^{67}Ga-citrate, as ^{67}Ga-citrate may also accumulate in non-HCC lesions such as abscess, metastases from adenocarcinomas and in lymphomatous disease (*24,26*). Other tumor-seeking agents, such as [^{75}Se]selenomethionine, ^{57}Co-bleomycin, rose bengal, HIDA or DISIDA were also found to be of limited value (*27–29*). New implications for imaging of HCC were introduced by Goldenberg et al. who reported a high sensitivity for iodine-labeled monoclonal antibodies raised against alpha-fetoprotein (AFP) (*30,31*). Whereas lower radioimmunoscanning sensitivities (*32*) were also reported since the original description (*30,31*), a comparative study of our NGA/insulin receptor scanning technique with immunoscintigraphy in patients with HCC may be a useful approach in the future.

In this study, we found that ^{123}I-Tyr-(A14)-insulin binds to the liver by a receptor-mediated process (*10,11*). The use of ^{123}I-Tyr-(A14)-insulin allows direct imaging of insulin binding to target organ sites and provides a new dimension to the in vivo study of insulin kinetics and metabolism. The rationale for using ^{123}I-Tyr-(A14)-insulin scanning to evaluate HCC was based on our observation that this radionuclide is taken up a 1000-fold more by HCC as opposed to normal liver tissue. The finding was verified through in vitro studies showing a higher number of specific binding sites for ^{123}I-Tyr-(A14)-insulin expressed on HCC.

We found that a defect detected on a NGA scan will show an accumulation in which the abnormality was due to HCC. Hepatocytes normally concentrate a large fraction of the injected dose of radiolabeled insulin because normal liver also contains insulin receptors. This also means that tumor imaging in the liver involves detection of increased uptake within normal liver uptake. Indeed, in 19 of our patients, HCC lesions had significantly increased HCC-to-normal liver ratios, but in 8 patients insulin uptake (binding) was not significantly different from the surrounding normal liver uptake and in 3 patients the HCC lesion showed decreased ^{123}I-Tyr-(A14)-insulin uptake. These differences in accumulation of ^{123}I-Tyr-(A14)-insulin is possibly explained by low numbers or absence of insulin receptors, coverage of insulin receptors by locally produced ligands or dedifferentiation of HCC cells. Such mechanisms may also be the reason for the decreased accumulation of ^{123}I-Tyr-(A14)-insulin reported in HCC lesions of Patients 11 and 14 (Table 1).

CONCLUSION

Our results indicate that combined use of ^{99m}Tc-NGA and ^{123}I-Tyr-(A14)-insulin could be helpful in the clinical diagnosis of human HCC. This dual-receptor-tracer methodology indicates sensitivity as well as specificity in the diagnosis of HCC. This method in combination with SPECT might provide distinct localization of HCC and could provide quick, noninvasive and safe identification of masses seen on US and/or CT.

ACKNOWLEDGMENTS

This study was supported in part by the Mayor of the City of Vienna and the Anton Dreyer Stiftung of the University of Vienna.

REFERENCES

1. Krenning EP, Bakker WH, Breeman WAP, et al. Localization of endocrine-related tumors with radioiodinated analogue of somatostatin. *Lancet* 1989; 1:242–244.
2. Virgolini I, Raderer M, Kurtaran A, et al. Vasoactive intestinal peptide receptor imaging in the localization of intestinal adenocarcinomas and endocrine tumors. *N Engl J Med* 1994;331:1116–1121.
3. Stockert JJ, Morell AG. Hepatic binding protein: the galactose receptor of mammalian hepatocytes. *Hepatology* 1983;3:750–757.
4. Vera DR, Stadalnik DR, Trudeau WL, Scheibe PO, Krohn KA. Measurement of receptor concentration and forward binding rate constant via radiopharmacokinetic modeling of ^{99m}Tc-galactosyl-neoglycoalbumin. *J Nucl Med* 1991;32:1169–1176.
5. Vera DR, Woodle ES, Stadalnik RC. Kinetic sensitivity of a receptor-binding radiopharmaceutical: technetium-99m-galactosyl-neoglycoalbumin. *J Nucl Med* 1991;30:1519–1530.
6. Virgolini I, Angelberger P, Müller C, et al. Technetium-99m-neoglycoalbumin binding to human hepatic binding protein. *Br J Clin Pharmacol* 1989; 29:207–212.
7. Virgolini I, Müller C, Klepetko W, et al. Decreased hepatic function in patients with liver metastases and hepatomas as monitored by ^{99m}Tc-galactosyl-neoglycoalbumin. *Br J Cancer* 1989;61:937–941.
8. Virgolini I, Müller C, Angelberger P, et al. Functional liver imaging with ^{99m}Tc-galactosyl-neoglycoalbumin (NGA) in alcoholic liver cirrhosis and fibrosis. *Nucl Med Commun* 1991;12:507–517.
9. Virgolini I, Müller C, Höbart J, et al. Liver function in acute viral hepatitis as determined by a hepatocyte-specific ligand: ^{99m}Tc-galactosyl-neoglycoalbumin. *Hepatology* 1992;15:593–598.
10. Hachiya HL, Treves ST, Kahn CR, Sodoyez JC, Sodoyez-Goffaux F. Altered insulin distribution and metabolism in Type I diabetics assessed by ^{123}I-insulin scanning. *J Clin Endocrinol Metab* 1986;64:801–807.
11. Sodoyez JC, Sodoyez-Goffaux F, Guillaume M, et al. Iodine-123-insulin metabolism in normal rats and humans. External detection by scintillation camera. *Science* 1983;219:865–867.
12. Sinclair AJ, Signore A, Bomanji J, Britton KE, Pozzilli P, Gale EAM. In vivo kinetics of ^{123}I-labeled insulin: studies in normal subjects and patients with diabetes mellitus. *Nucl Med Commun* 1987;8:779–786.
13. Koontz JW, Iwahashi M. Insulin as a potent, specific growth factor in rat hepatoma cell line. *Science* 1981;211:947–949.
14. Massague J, Blinderman LA, Czech MP. The high affinity insulin receptor mediates growth stimulation in rat hepatoma cells. *J Biol Chem* 1982;257: 13958–13963.
15. Simonetti RG, Camma C, Fiorello F, Politi F, D'Amico G, Pagliaro L. Hepatocellular carcinoma. *Dig Dis Sci* 1993;36:962–972.
16. Bohring CC, Squires TS, Tong T. Cancer statistics 1993. *CA Cancer J Clin* 1993;43:7–26.
17. Liang TJ, Jeffers LJ, Reddy KR et al. Viral pathogenesis of hepatocellular carcinoma in the United States. *Hepatology* 1993;18:1326–1333.
18. Tsai JF, Chang WY, Jeng JE, Ho MS, Lin ZY, Tsai JH. Effects of hepatitis C and B viruses infection on the development of hepatocellular carcinoma. *J Med Virol* 1994;44:92–95.
19. De-Bac C, Stroffolini T, Gaeta GB, Taliani G, Giusti G. Pathogenetic factors in cirrhosis with and without hepatocellular carcinoma: a multicenter Italian study. *Hepatology* 1994;20:1225–1230.
20. Bennett WE, Bova JG. Review of hepatic imaging and a problem-oriented approach to liver masses. *Hepatology* 1990;12:761–775.
21. Virgolini I, Yang Q, Li SR, et al. Cross-competition between vasoactive intestinal peptide and somatostatin for binding to tumor cell membrane receptors. *Cancer Res* 1994;54:690–700.
22. Scatchard G. The attractions of proteins for small molecules and ions. *Ann NY Acad Sci* 1949:660–672.
23. Cornelius EA, Atterbury CE. Problems in the imaging diagnosis of hepatomas. *Clin Nucl Med* 1984;9:30–38.
24. Lee VE, O'Brien MJ, Morris PM, Devereux DF, Shapiro JH. The specific diagnosis of hepatocellular carcinoma by scintigraphy. *Cancer* 1984;56: 25–36.
25. Lomas F, Dibos PE, Wagner HN. Increased specificity of liver scanning with the use of gallium-67 citrate. *N Engl J Med* 1972;16:949–951.
26. Bekerman C, Hoffer PB, Bitran JD. The role of gallium-67 in the clinical evaluation of cancer. *Semin Nucl Med* 1985;15:72–103.
27. Calvet X, Pons F, Bruix J, et al. Technetium-99m DISIDA hepatobiliary agent in diagnosis of hepatocellular carcinoma relationship between detectability and tumor differentiation. *J Nucl Med* 1988;29:1916–1920.
28. Kew MC, Geddes EW, Levin J. False-negative ^{75}Se-methionine scans in primary liver cancer. *J Nucl Med* 1974;15:234–241.
29. Kew MC, Allan J, Levin J. Cobalt-57-bleomycin as a tumor scanning agent in primary hepatocellular cancer. *J Nucl Med* 1976;1:234–239.
30. Goldenberg DM, Goldenberg H, Higgenbotham E, Shochat D, Ruoslahti E. Imaging of primary and metastatic liver cancer with ^{131}I monoclonal and polycloncal antibodies against alphafetoprotein. *J Clin Oncol* 1987;5:1827–1835.
31. Kim EE, DeLand FH, Nelson MO, et al. Radioimmunodetection of cancer with radiolabeled antibodies to alpha-fetoprotein. *Cancer Res* 1980;40:3008–3012.
32. Demangeat JL, Manil L, Demangeat C, et al. Is anti-alpha-fetoprotein immunoscintigraphy a promising approach for the diagnosis of hepatoma? *Eur J Nucl Med* 1988;14:612–620.

EDITOR'S NOTE: This article was incorrectly placed within the Laboratory Studies section; it should have appeared within the Human Studies section.